Coupling Capacitively Distinct Mechanical Resonators for Room-Temperature Phonon-Cavity Electromechanics

Alok Pokharel, Hao Xu, Srisaran Venkatachalam, Eddy Collin, Xin Zhou

▶ **To cite this version:**

Alok Pokharel, Hao Xu, Srisaran Venkatachalam, Eddy Collin, Xin Zhou. Coupling Capacitively Distinct Mechanical Resonators for Room-Temperature Phonon-Cavity Electromechanics. Nano Letters, 2022, 22 (18), pp.7351-7357. 10.1021/acs.nanolett.2c01848 . hal-03651266

HAL Id: hal-03651266
https://hal.science/hal-03651266v1

Submitted on 15 Sep 2022

HAL is a multi-disciplinary open access archive for the deposit and dissemination of scientific research documents, whether they are published or not. The documents may come from teaching and research institutions in France or abroad, or from public or private research centers.

L'archive ouverte pluridisciplinaire **HAL**, est destinée au dépôt et à la diffusion de documents scientifiques de niveau recherche, publiés ou non, émanant des établissements d'enseignement et de recherche français ou étrangers, des laboratoires publics ou privés.

Coupling capacitively distinct mechanical resonators for room temperature phonon-cavity electromechanics

Alok Pokharel,[†] Hao Xu,[†] Srisaran Venkatachalam,[†] Eddy Collin,[‡] and Xin Zhou[*,†]

[†] *Univ. Lille, CNRS, Centrale Lille, Univ. Polytechnique Hauts-de-France, UMR 8520 - IEMN, F-59000 Lille, France*

[‡] *Univ. Grenoble Alpes, Institut NEEL - CNRS UPR2940, 25 rue des Martyrs, BP 166, 38042 Grenoble Cedex 9, France*

E-mail: CorrespondingAuthor:xin.zhou@cnrs.fr

Abstract

Coupled electromechanical resonators that can be independently driven/detected and easily integrated with external circuits are essential for exploring mechanical modes based signal processing and multifunctional integration. One of the main challenges lies in controlling energy transfers between distinct resonators experiencing nano-scale displacements. Here, we present a room temperature electromechanical system that mimics a "phonon-cavity", in analogy with optomechanics. It consists in a silicon nitride membrane capacitively coupled to an aluminum drum-head resonator. We demonstrate electromechanically induced transparency and amplification through manipulating the mechanical displacements of this coupled system, creating interferences in the measured signal. The anti-damping effects, generated by phonon-cavity force,

have been observed in both movable objects. We develop an analytical model, which captures the analoguous optomechanical features in the classical limit and enables to fit quantitatively the measurements. Our results open up new possibilities for building compact and multifunctional mechanical systems, and exploring phonon-phonon coupling based optomechanics.

Keywords

phonon-cavity, coupled mechanical resonators, membrane, transparency and amplification, interference

Micro- and nano-electromechanical systems, allowing mechanical displacements to couple with electrical and optical signals, are extensively studied for various applications and fundamental research.[1,2] The specific features of tiny scale and high quality factor resonances are attractive for sensing applications.[3–6] Their intrinsic nonlinearity and mechanical transduction design have been implemented for developing logic gates,[7,8] radio frequency (RF) amplifiers[9] and memory nodes.[10] In recent years, the study of mode coupling, which exists between different mechanical modes in a single system but also between different resonators, attracts great research interests. Because they allow to transmit information between mechanical modes[11,12] and to filter signals in different frequency bands through controlling transfers of energy.[13] In addition to these applied possibilities, such devices can also be viewed as model systems to implement mechanical analogues of some other phenomena.[14]

As such, one of the successful examples exploiting mechanical mode coupling is the concept of "phonon-cavity",[15,16] inspired by recent achievements in optomechanics. Optomechanics, which studies interactions between the mechanical vibrations and photons confined in a cavity, offers a powerful platform for many engineering applications, from sensing (e.g. detecting thermal Brownian motion) to the generation of mechanical self-sustained oscillations, and even the storage of light.[17–19] In order for the two coupled mechanical modes to exploit the rich physics available with optomechanics, the phonon-cavity scheme is built by

implementing the mode with the higher resonance frequency Ω_1 as a phonon cavity in analogy with the optical/microwave one, and then pumping it with a signal at frequency $\sim \Omega_1 \pm \Omega_2$. Here, Ω_2 is the resonance frequency of the other mode. The concept of phonon-cavity not only enables the two coupled mechanical modes to inherit those interesting functions of optomechanics, but also further enriches existing optomechanical applications, in both classical and potentially the quantum regime.[16,20–22]

Up to now, in most phonon-cavity schemes, the coupling is created between different mechanical modes with a single resonator by means of an intrinsic nonlinearity, or between different resonators by using physical connections to transmit a displacement-induced tension.[3,11,16,23–25] However, mechanical coupling design yields implementation complexities in optimizing the coupling between distinct and distributed resonators, and poses a challenge for electromechanical devices desiring higher resonance frequencies and flexible tunability. Compared to mechanical coupling designs, electrostatic coupling schemes are widely implemented in diverse electrical integrated systems. It allows to implement the coupling of distributed resonators experiencing nano-scale displacements, but also to drive/detect independently each resonator of the coupled system.[26,27] However, it is still challenging to achieve directly coupled distinct mechanical resonators via capacitive coupling, especially for compact schemes.

In this work, we present coherent energy transfers between two capacitively coupled and distinct electromechanical resonators, consisting of an Al drum suspended on top of a SiN membrane drum. Both resonators can be driven and detected independently. We explore phonon-cavity electromechanics based on a simple theoretical model which is analogous to optomechanics. At room temperature (RT), we experimentally demonstrate electromechanically induced transparency and amplification of the input signal through controlling the electromechanical energy transfers (in the form of phonons) to create signal interferences in the coupled system. We observe mechanical anti-damping effects (with respect to the applied driving tone) in both coupled drums generated by the phonon-cavity force, exhibiting the

trend expected by the theoretical model. These results indicate that this new type of device design could serve for phonon-based information processing in both classical and quantum regimes, and is potentially useful for building multifunctional compact mechanical systems.

The device structure investigated in this work consists of two distinct electromechanical resonators. One of them is a silicon nitride (SiN) circular membrane nanomechanical resonator, $\approx$ 80 nm in thickness and $\approx$ 36 μm in diameter, covered with an aluminum (Al) thin film $\approx$ 25 nm in thickness, which has been fabricated from a silicon substrate covered with a stoichiometric SiN thin film, $\sim$ 1 GPa tensile stress. The other resonator is an Al drum having a diameter of $\approx$ 40 μm suspended on the top of a SiN membrane. Its mechanical property approaches to a plate model (details in SI), as shown in Figure 1 (a). The measurement setup is schematically depicted in Figure 1 (b). Mechanical motions of both electromechanical resonators can be independently excited by passing RF signals V_{ac} combined with *dc* voltages V_{dc} to generate an electrostatic driving force. All the measurements are performed at RT, under vacuum ($\sim 10^{-6}$ mbar) to minimize air damping. Figure 1 (c) shows linear responses of both Al drum and SiN drum resonators, for their fundamental modes. For the Al drum, the resonance frequency is $\Omega_{Al}/(2\pi) \approx 2.95$ MHz with a quality factor $Q_{Al} \approx 358$. A finite element simulation is consistent with a low tensile stress in the Al film $\sim$40 MPa. The SiN drum, a high-stress thin membrane, vibrates at high frequency $\Omega_{SiN}/(2\pi) \approx 11.792$ MHz with a high quality factor $Q_{SiN} \approx 1.8\times10^4$. In the experiment, we take the SiN nanomechanical resonator as a phonon cavity, as $\Omega_{SiN} > \Omega_{Al}$. It presents an energy leaking rate much smaller than that of the coupled Al drum, thus contrary to standard optomechanical systems.

Electromechanical capacitive coupling model. The whole device structure can be viewed as a parallel plate capacitor $C_g\left(X_1, X_2\right)$, where each plate is a membrane drum resonator, as shown in Figure 1 (a). The mechanical displacement of each membrane is described by $X_1(t)$ and $X_2(t)$ resonating at the frequency Ω_1 and Ω_2 respectively far from each other, with $\Omega_1 > \Omega_2$. Driven by the electrostatic force $F_{1,2}(t) = \frac{[V_{dc}+V_{ac}(t)]^2}{2}\frac{\partial}{\partial X_{1,2}}C_g\left[X_1\left(t\right), X_2\left(t\right)\right]$,

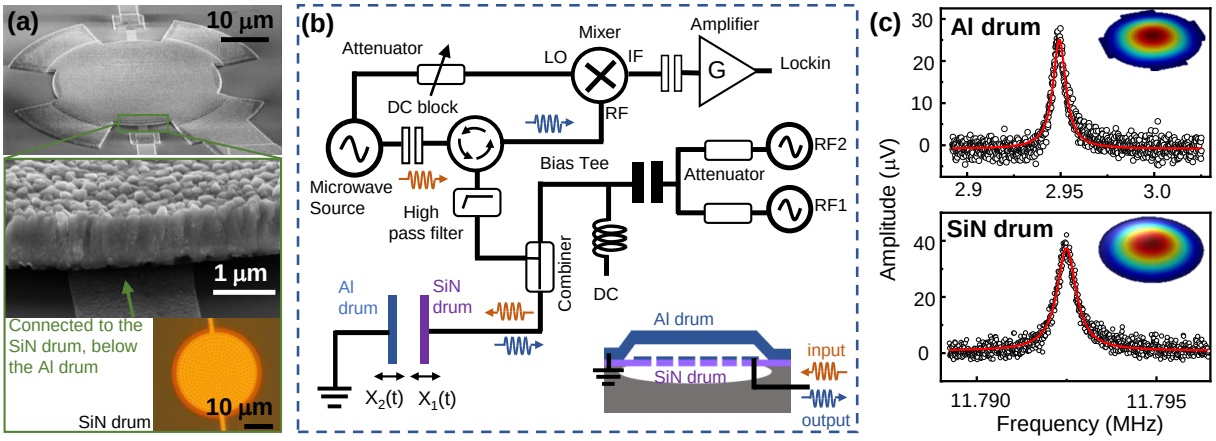

Figure 1: (a) Above, a scanning electron microscope (SEM) image of an Al drum resonator, $\approx$ 550 nm in thickness, which is suspended on top of a SiN circular membrane covered with an Al thin film.[28] The Al drum is designed to have a "X"-shaped clamping structure covering $\sim$50% of the circumference. Below, a magnified SEM image of the vacuum gap region marked by the green box in the above image. The distance between the Al drum and the SiN one is $d \approx 600$ nm. At the bottom, an optical image of a SiN drum resonator covered with an Al thin film, before the Al drum was fabricated on top of it. There is no physical connection between the two drums. More details of device fabrication are shown in SI: Device fabrication and basic mechanical properties (b) Schematic diagram of the measurement setup. Both electromechanical resonators are driven by low frequency signals combined with RF and *dc* signals. The mechanical displacement is imprinted in the reflected microwave signals and read out by a lockin amplifier through frequency down-conversion.[28] The inset schematic shows a cross-sectional view of the device structure. (c) Linear resonance response of the Al drum resonator (upper) and SiN drum resonator (lower), which are measured at V_{dc}=2 V, V_{ac}=2 mV_p and 0.2 mV_p respectively. The inset figures show the corresponding mechanical mode shapes obtained from finite element simulations.

we therefore model these two capacitively coupled drums in the linear response regime via the following coupled equations of motion for the displacements $X_1(t)$ and $X_2(t)$,

$$\begin{aligned}\ddot{X}_1 + \gamma_1\dot{X}_1 + \Omega_1^2 X_1 &= \frac{V_{ac}V_{dc}}{m_1\, d}C_{g0}\left[1 - \frac{2(X_2 - X_1)}{d}\right], \\ \ddot{X}_2 + \gamma_2\dot{X}_2 + \Omega_2^2 X_2 &= \frac{V_{ac}V_{dc}}{m_2\, d}C_{g0}\left[-1 + \frac{2(X_2 - X_1)}{d}\right].\end{aligned} \tag{1}$$

Here, $\gamma_{1,2}$ are the mechanical damping rates and $m_{1,2}$ are the effective masses of each drum. The driving force, acting on a simple parallel plate capacitor, is truncated at the second order in a Taylor expansion, and C_{g0} is the initial capacitance between the two membranes separated by a distance d. In Eq.1, the approximation $2V_{dc}V_{ac} + V_{ac}^2 \approx 2V_{dc}V_{ac}$ has been made by considering the typical situation encountered in measurements: $V_{dc} \gg |V_{ac}|$. The static contribution V_{dc}^2 has been dropped of the equation since it cannot drive resonantly the modes. Following the concept of cavity optomechanics, the mechanical resonator having the higher resonance frequency in the coupled system is chosen as the phonon-cavity. In a two-tone driving scheme, we exploit one driving tone with frequency Ω_d to weakly probe one of the coupled membranes around its resonance frequency (Ω_1 or Ω_2), and the other tone with frequency Ω_p to pump the phonon-cavity at its sideband $\sim \Omega_1 \pm \Omega_2$. The V_{ac} carrying the two tones therefore can be written in the form $V_{ac}\,(\Omega_p, \Omega_d) = \frac{\mu_p}{2}e^{-i\Omega_p t} + \frac{\mu_d}{2}e^{-i\Omega_d t} + c.c.$ The μ_p and μ_d are complex amplitudes corresponding to the $V_{ac}\,(\Omega_p)$ and the $V_{ac}(\Omega_d)$ components, respectively. Eq.1 is solved in the rotating frame through looking for the mechanical displacement $X_{1(2)}(t)=\frac{x_{1(2)}(t)}{2}e^{-i\Omega_d t} + c.c$ mainly driven by the probe signal, and the displacement $X_{2(1)}(t)$ also depends on the interaction between the probe tone and the pump tone. The $x_{1,2}$ are the slowly varying complex amplitudes of the mechanical displacement, corresponding to each membrane's motion. In analogy with microwave optomechanics, we define the coupling strength between the phonon-cavity (SiN membrane, with index 1) and its coupled Al drum (with index 2) as $G = \frac{\partial\Omega_1}{\partial X_2}$ and the single phonon coupling strength $g_0{=}G\sqrt{\frac{\hbar}{2m_2\Omega_2}}$, where $\sqrt{\frac{\hbar}{2m_2\Omega_2}}$ is the zero-point fluctuations of the mechanical mode indexed

2 with resonance frequency Ω_2. While the experiment is by no means anywhere close to the quantum regime, we introduce this language as a commodity for a direct comparison with the usual formalism of optomechanics. We first consider a two-tone driving scheme, which has been generally investigated in optomechanics. The phonon-cavity is probed with a frequency Ω_d=$\Omega_1 + \delta$ and is pumped at the frequency Ω_p=$\Omega_1 \pm \Omega_2 + \Delta$. The δ parameter is therefore a frequency detuning from frequency Ω_1 for the probe tone. The Δ parameter is a frequency detuning for the pump, from the frequency $\Omega_1 \pm \Omega_2$. Solving Eq.1, the probed mechanical displacement x_1 is given by

$$x_1 = \frac{f_d}{2m_1\Omega_1}\frac{1}{\chi_1^{-1} \pm n_p g_0^2 \chi_2}, \tag{2}$$

where n_p=$\frac{2|f_p|^2}{m_1\Omega_1^2}\frac{1}{\hbar\Omega_p}$ is the phonon number generated by the pumping force f_p=$\frac{C_{g0}V_{dc}\mu_p}{d}$ and $f_d = \frac{C_{g0}V_{dc}\mu_d}{d}$ is the driving force generated by the probe signal. Both f_d and f_p are complex amplitudes. The $\chi_1 = \frac{1}{-\delta - i\frac{\gamma_1}{2}}$ and $\chi_2 = \frac{1}{\Delta - \delta - i\frac{\gamma_2}{2}}$ are susceptibilities of the phonon-cavity and the coupled electromechanical resonator. The "-" and "+" symbols in Eq.2 correspond to a "red" or "blue" sideband pumping scheme, respectively. Similarly, the probe tone can be applied at $\Omega_d = \Omega_2 + \delta$ in order to excite the Al drum response.

The probed mechanical displacement exhibits a behavior similar to optomechanically induced transparency and amplification.[19,29] In this two-tone scheme, the mechanical interactions can be decomposed into two coherent steps for transfers of energy (in the form of phonons) between two coupled resonators, as indicated in the Figure 2(a) and 2(b), where each graph corresponds to one of our two different probing cases. In a first step, the probe and pump tone create a phonon-cavity force acting on the unprobed membrane that excites its mechanical vibrations, corresponding to the process $< 1 >$ in the Figure 2(a) and 2(b). Then, these generated mechanical phonons are fed back to the probed resonator, corresponding to the process $< 2 >$. An interference therefore is built between these phonons described by the term $n_p g_0^2 \chi_2$ acting on the unprobed membrane in Eq. 2 and the initial probe sig-

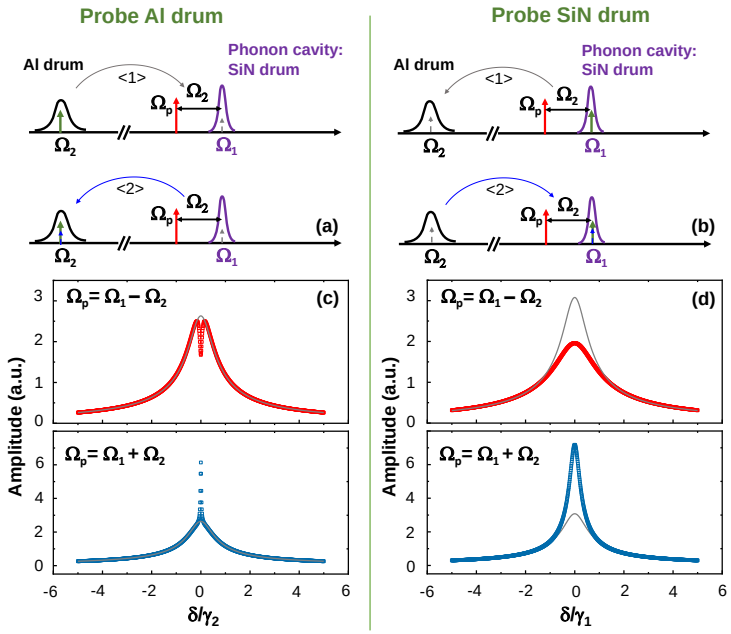

Figure 2: Diagram of the red sideband pumping scheme of the phonon-cavity SiN drum Ω_p=Ω_1-Ω_2+Δ, while probing (a) the Al drum at frequency Ω_d= $\Omega_2+\delta$ and (b) the SiN drum at frequency Ω_d= $\Omega_1+\delta$. For a blue sideband pumping scheme Ω_p=Ω_1+Ω_2+Δ, the Ω_p arrow therefore is above Ω_1, detuned by Ω_2 (not shown). $<1>$ corresponds to the probe and the pump tone frequency up-conversion process in (a) and down-conversion process in (b), which excites the un-probed mechanical vibrations marked as dashed grey arrows. $<2>$ feed back process of the generated phonons, corresponding to the frequency down-conversion process in (a) and up-conversion process in (b). An interference is created between these fed back phonons marked as dashed blue arrows and the initial probe signal marked with green arrows. Simulated mechanical response of (c) the Al drum and (d) the SiN drum, corresponding to the red and blue sideband pumping of the phonon cavity (see Ω_p in legend). Details of formula derivation are shown in the SI. The gray curves are the mechanical responses when there is no pump tone, n_p=0. Both blue and red curves are computed with $n_p g_0^2$=$\gamma_2\gamma_1/7$, $f_d/(2m_2\Omega_2)$= $f_d/(2m_1\Omega_1)$, and Δ=0. Besides, we also consider $\gamma_{Al} \sim 10\,\gamma_{SiN}$ in all simulated mechanical responses, including the case of no pump tone.

nal corresponding the term χ_1. This interference can be destructive or constructive, which depends on pumping the cavity at its red or blue sideband. Impacts of this interference on the resonance peaks measured with the two probe configurations are illustrated in Figure 2(c) and 2(d), taking taking into account the fact that the phonon cavity linewidth γ_{SiN} is about two orders smaller than that of the coupled Al drum (our experimental conditions). As indicated in Eq.2, the linewidth of the unprobed mechanical resonator determines the frequency bandwidth of the transparency and amplification effects. For instance, when the phonon-cavity is red sideband pumped, the Lorentzian curve of the Al drum mechanical response exhibits a narrow dip inside its lineshape due to the fact $\gamma_{SiN} < \gamma_{Al}$, as shown in Figure 2(c). On the contrary, the probed signal propagating through the SiN drum is fully suppressed, as the γ_{Al} determines the linewidth of the transparency window. This phenomenon is quite different from conventional optomechanical systems in which the mechanical damping rate is usually much smaller than that of the coupled cavity. These results demonstrate that both transparency and amplification windows can be controlled through engineering the mechanical damping rate in the phonon-cavity system.

Electromechanically induced transparency and amplification. In order to build the interference process, one of the key points is that the unprobed mechanical resonator should provide enough phonons to be fed back by the pump tone, generating the interference with the initial probe tone. The motion equation Eq.1 indicates that the energy transferred between the two movable membranes is determined by the effective pumping force $f_p\frac{X_{1(2)}(t)}{d}$, when the probe tone is driving the mechanical displacement $X_{1(2)}(t)$ around its resonance frequency $\Omega_{1(2)}$. Therefore, the probe tone should have a large amplitude $V_{ac}(\Omega_d)$ in order to increase the pump efficiency and provide a large number of phonons for the interference process. To demonstrate it, the phonon-cavity is red sideband pumped at a frequency $\Omega_p/2\pi$=$\Omega_1/2\pi - \Omega_2/2\pi + \Delta$ using Δ=-2.5 kHz with a fixed pump amplitude $V_{ac}(\Omega_p) = 100$ mV_p and $V_{dc} = 2$ V. Figure 3 shows the linear response of the Al drum probed by different $V_{ac}(\Omega_d)$, as a function of the frequency detuning δ. At the largest drive amplitudes, a clear

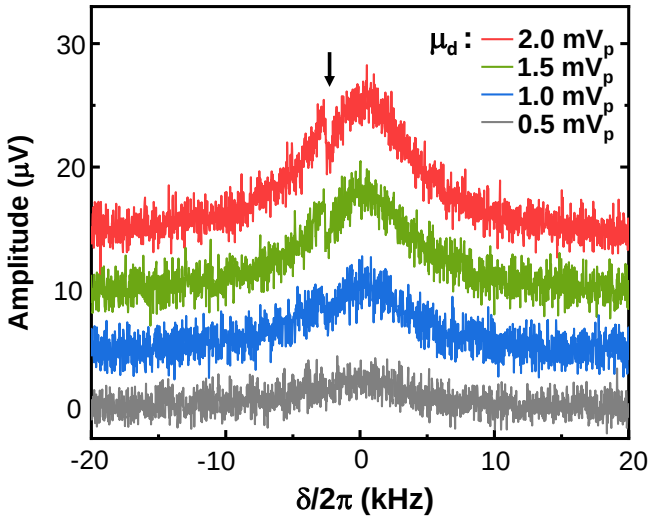

Figure 3: Mechanical response of the Al drum when the phonon-cavity is pumped at its red sideband at a frequency $\Omega_p/2\pi = \Omega_1/2\pi - \Omega_2/2\pi - 2.5$ kHz with an ac pump amplitude $V_{ac}(\Omega_p) = 100$ mV_p. These curves were measured with different probe ac voltages μ_d applied to the Al drum, from 0.5 mV_p to 2.0 mV_p. The δ is the probe frequency detuning from the resonance frequency of Al drum, $\Omega_d = \Omega_2 + \delta$. When the detuning δ matches Δ = -2.5 kHz, a clear dip is visible (arrow, see text).

dip is visible when the two detunings are matched, $\delta = \Delta$.

Electromechanical responses of these coupled resonators have been measured as a function of the pump tone detuning Δ and the probe frequency detuning δ, for both red and blue sideband pumping schemes, as shown in Figure 4(a)-4(d). These measurement results clearly indicate that the linewidth of the interference window corresponding to the pump tone tuning Δ is related to the unprobed membrane. This is because the unprobed membrane in the coupled system acts as a phonon transfer station. Within the bandwidth of the unprobed resonator, phonons can be generated from the interaction between the pump and the probe tone and can coherently create constructive or destructive interferences with the probe tone. Figure 4(c) and 4(d) show the simultaneous measurement results of the electromechanical responses of the probed and the unprobed membranes, in which the phonon-cavity is driven at a frequency Ω_d=$\Omega_1 + \delta$ and is pumped at its blue sideband Ω_p=$\Omega_1 + \Omega_2 + \Delta$. Figure 4(c) clearly shows a constructive interference result as the probed signals have been amplified

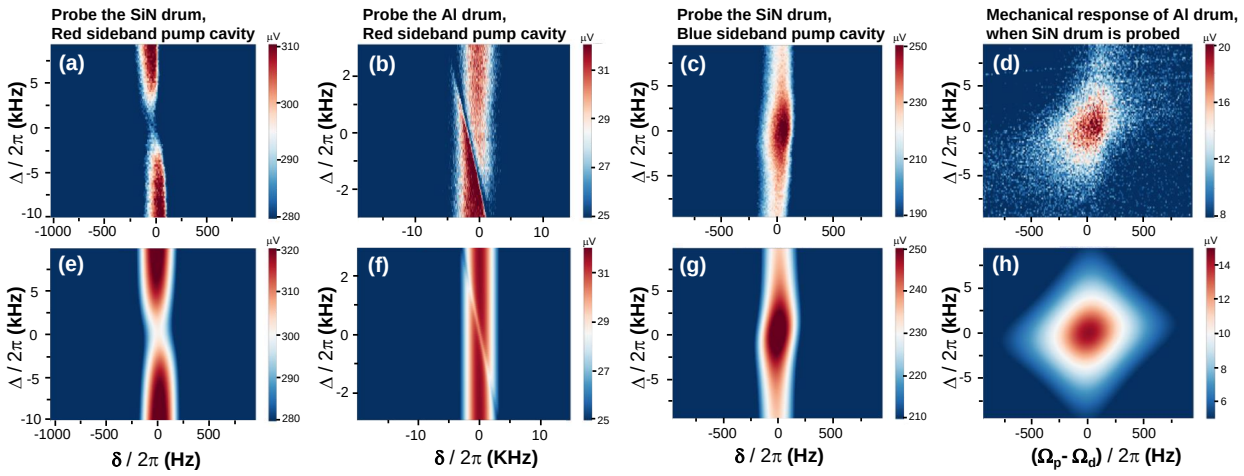

Figure 4: Electromehanically induced transparency and amplification in two capacitively coupled membranes. In a red sideband pumping scheme, (a) electromechanical response of the phonon-cavity measured with driving amplitudes $V_{dc} = 4$ V, $V_{ac}(\Omega_d) = 1$ mV$_p$, $V_{ac}(\Omega_p) = 70$ mV$_p$, and probed at $\Omega_d = \Omega_1 + \delta$; (b) mechanical response of the Al drum measured with driving amplitudes $V_{dc} = 2$ V, $V_{ac}(\Omega_d) = 3$ mV$_p$, $V_{ac}(\Omega_p) = 100$ mV$_p$, and probed at $\Omega_d = \Omega_2 + \delta$. In a blue sideband pumping scheme, (c) the phonon-cavity response obtained with driving amplitudes $V_{dc} = 4$ V, $V_{ac}(\Omega_d) = 0.7$ mV$_p$, $V_{ac}(\Omega_p) = 70$ mV$_p$, and probed at $\Omega_d = \Omega_1 + \delta$; (d) simultaneously measured the corresponding spectra at the frequency $\Omega_p - \Omega_d$. The spectra correspond to the process $< 1 >$ marked in Figure 2 (b), in a blue sideband pumping scheme. The Δ is the frequency detuning regarding the pump tone, with Ω_p=$\Omega_1 \pm \Omega_2$+Δ for a red or blue sideband pumping scheme. (e)-(h) Simulation results for the measurements shown in (a)-(d), which were performed by using the theoretical model described in Eq.1 and all experimental parameters mentioned above.

within the interference window and the Figure 4(d) indicates phonon generation (displacements in the nano-meter scale) in the mechanical mode of the Al drum. The mechanical displacements of both membranes $X_{1(2)}$, corresponding to different driving and pumping schemes, have been calculated based on the capacitive coupling model described by Eq. 1. The calculated mechanical displacements are converted into electrical signal amplitude in a microwave measurement scheme and are shown in Figure 4(e)-(h), by using the relation $V_{out} = \omega Z_0 C_{g0} X_{1(2)} V_{\mu w}/(2d)$.[28] Here, ω and $V_{\mu w}$ are the frequency and the amplitude of the microwave signal for detection, respectively. The parameter Z_0 is the impedance of the measurement chain (here, 50 Ohm). The measurement results have been quantitatively fitted within ∼10% error bar by taking effective masses for the SiN membrane of $m_1 \approx 4.4\times10^{-14}$ kg and for the Al drum of $m_2 \approx 4.41\times10^{-13}$ kg, and by using the experimental parameters mentioned above.

Besides, we also evaluate the maximum coupling rate $g = g_0\sqrt{n_p}$ by taking the largest pump force performed in this measurement, which has been generated by applying V_{dc} = 4 V and $V_{ac}(\Omega_p)$ = 70 mV_p. It gives $g \approx 1024$ rad/s , which remains smaller than $\gamma_{SiN} = \Omega_{SiN}/Q_{SiN}$ and $\gamma_{Al} = \Omega_{Al}/Q_{Al}$. It means that the pumping force does not provide enough phonons to drive the coupled mechanical system into the so-called strong coupling regime.[11,26] In the present RT measurement, the pumping force is mainly limited by the large thermal background noise due to the heating effects brought in by the high pumping power. On the contrary, in the cryogenic temperature range, this limitation will be greatly suppressed. In addition, the typical damping rates of both SiN and Al mechanical resonators are $\sim10^2$ Hz in mK range with resonance frequencies in the MHz range,[30,31] which could allow this device to access the strong coupling regime.

Phonon-cavity force effects on mechanical damping rate. In optomechanical systems, the cavity force has been implemented to decrease mechanical damping rate in order to improve sensing resolutions, through pumping the coupled cavity at its sideband.[32] Our device gives more degrees of freedom and provides an opportunity to observe the cavity

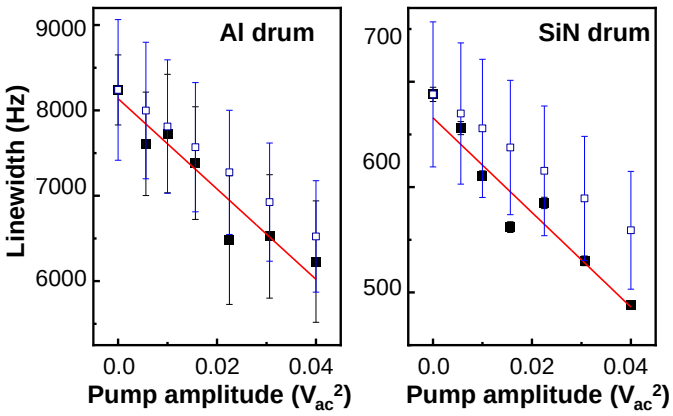

Figure 5: In a blue sideband pumping scheme $\Omega_p = \Omega_1 + \Omega_2$, the linewidth of the Al drum and the SiN drum are decreasing as a function of the *ac* pump power $[V_{ac}^2(\Omega_p)]$, as shown in black squares. The dc bias is $V_{dc} = 4$V, the probing voltage $V_{ac}(\Omega_d) \approx 500\ \mu V$ for the Al drum and the probing voltage $V_{ac}(\Omega_d) \approx 200\ \mu V$ for the SiN drum. Red lines are linear fits of the data (see text). The white squares with blue edges are calculation results based on our model and experimental parameters mentioned above. There is a small offset between the measurement and calculation results, which could be induced from inaccuracy in the device parameters, e.g. d, m_1, and m_2.

force acting on both resonators, including the one acting as a phonon-cavity. Here, we exploit a large *ac* signal to pump the blue sideband of the phonon-cavity, and apply a small *ac* one to respectively excite mechanical displacements of the SiN or Al drum to be just above the noise floor of the measurement chain. As shown in Figure 5, the linewidth of both coupled membranes decreases with increasing the pump power (V_{ac}^2), exhibiting the typical "optical anti-damping effect".[33] We can use a single-tone driving scheme to model this effect in two capacitively coupled membranes based on Eq. 1, in which the phonon cavity is pumped at the frequency $\Omega_1 + \beta$. Here, the β is a global frequency detuning, with $\beta \sim \Omega_2$ for the blue sideband and $\beta \sim -\Omega_2$ for the red sideband. The sideband scheme pumping the cavity gives rise to two satellite signals, corresponding to Stokes- and anti-Stokes scattering.[34] The mechanical susceptibility is altered due to the phonon-cavity force generated by interactions between the pump tone and these generated Stokes and anti-Stokes processes, yielding modulations of the mechanical damping rates.[33,34] By employing a similar approach as the one applied to the electric circuit modeling of microwave optomechanics,[34]

we therefore deduce the additional damping term γ_{2opt} of the Al drum (with index 2) due to the back-action force of the phonon-cavity, but also the additional damping term γ_{1opt} for the phonon-cavity (see details in SI), as shown in Eq.3. The additional damping terms make the initial mechanical damping rate $\gamma_{1(2)}$ become $\gamma_{1(2)eff}$=$\gamma_{1(2)}$+$\gamma_{1(2)opt}$,

$$\begin{aligned}
\gamma_{2opt} &= \frac{|f_p|^2}{4m_1m_2\,d^2\,\Omega_1\Omega_2}\left[\frac{\gamma_1}{(\Omega_2+\beta)^2+\frac{\gamma_1^2}{4}}-\frac{\gamma_1}{(\Omega_2-\beta)^2+\frac{\gamma_1^2}{4}}\right], \\
\gamma_{1opt} &= \frac{|f_p|^2}{4m_1m_2\,d^2\,\Omega_1\Omega_2}\left[\frac{\gamma_2}{(\Omega_2-2\Omega_1-\beta)^2+\frac{\gamma_2^2}{4}}-\frac{\gamma_2}{(\Omega_2-\beta)^2+\frac{\gamma_2^2}{4}}\right].
\end{aligned} \tag{3}$$

In our measurement of a blue sideband pumping scheme with β=Ω_2, Eq.3 demonstrates the fact that the effective damping rate of the Al drum γ_{2eff} is inversely proportional to the initial damping rate of the coupled phonon-cavity, γ_1, in accordance with the "optical damping effect" in an optomechanical system. While conversely, for the damping rate of the phonon-cavity, γ_{1eff} is $\propto 1/\gamma_2$. If we consider the experimental condition $\Omega_{SiN}, \Omega_{Al} \gg \gamma_{SiN}$, γ_{Al}, Eq. 3 leads to $\gamma_{1eff}/\gamma_{2eff} \approx \gamma_1/\gamma_2$. In our measurement, slopes of the linewidth versus V_{ac}^2 can be obtained from the linear fit of the measurement results shown in Figure 5, for both membranes. The ratio between these slopes gives ≈11.8, which is in extremely good agreement with the value of γ_{SiN}/γ_{Al} ≈12.0 expected from our analytic model.

In conclusion, we have built a "phonon-cavity" optomechanical analogue, made of two distinct electrostatically coupled nano-mechanical resonators. Following the concept of phonon-cavity, we manipulate the electromechanical energy transfer between the modes (in the form of phonons) to create destructive or constructive interferences that control the signal propagation, leading to electromechanically induced transparency and amplification. By exploiting sideband pumping techniques, anti-damping effect has also been demonstrated in both coupled mechanical objects, which is potentially useful for sensing applications. This device scheme is compact for integration and manipulations, which could make it an ideal platform for exploring phonon based multi-function systems through combining signal processing and sensing functions, and enriching optomechanical systems. Besides, parametric coupling

model is built, which captures optomechanical features and provides theoretical analyses that quantitatively fit our measurement results. These investigations establish connections between a setup with two directly coupled movable objects and a standard optomechanical system in the classical regime that can be further extended to other parametrically coupled systems (e.g. electrical circuit modeling of optomechanics[34]) and be developed to facilitate today's quantum engineering.[19,21]

Acknowledgement

X.Z. conceived the design of the experiment. A.P. collected data, H.X. participated theoretical modeling, S.V. fabricated the device. X.Z built the setup, performed the measurements, and developed the analytic model. X.Z. wrote the manuscript. All authors contributed to scientific discussions and corrections of the manuscript. Both E.C. and X.Z. supervised the project.

We would like to acknowledge support from the STaRS-MOC project No. 181386 from Region Hauts-de-France (X.Z.), the project No. 201050 from ISITE-MOST (X.Z.), the ERC CoG grant ULT-NEMS No. 647917 (E.C.). The research leading to these results has received funding from the European Union's Horizon 2020 Research and Innovation Programme, under grant agreement No. 824109, the European Microkelvin Platform (EMP). This work was partly supported by the French Renatech network and RF-MEMS platform in IEMN. The authors acknowledge SMMiL-E, IRCL, and Contrat de Plan Etat-Région CPER Cancer 2015-2020 for technical support on wire bonding.

Supporting Information Available

- Filename: Device fabrication and basic mechanical properties
- Filename: Analytical calculation for two-tone driving scheme

- Filename: Analytical calculation for single-tone sideband pumping scheme: analogy to optomechanical damping effect

References

(1) Lyshevski, S. E. *MEMS and NEMS: systems, devices, and structures*; CRC press, 2018.

(2) Bachtold, A.; Moser, J.; Dykman, M. Mesoscopic physics of nanomechanical systems. **2022**, arXiv:2202.01819. arXiv.org e-Print archive. https://doi.org/10.48550/arXiv.2202.01819.

(3) Spletzer, M.; Raman, A.; Wu, A. Q.; Xu, X.; Reifenberger, R. Ultrasensitive mass sensing using mode localization in coupled microcantilevers. *Applied Physics Letters* **2006**, *88*, 254102.

(4) Spletzer, M.; Raman, A.; Sumali, H.; Sullivan, J. P. Highly sensitive mass detection and identification using vibration localization in coupled microcantilever arrays. *Applied Physics Letters* **2008**, *92*, 114102.

(5) Yang, Y.-T.; Callegari, C.; Feng, X.; Ekinci, K. L.; Roukes, M. L. Zeptogram-scale nanomechanical mass sensing. *Nano letters* **2006**, *6*, 583–586.

(6) Chaste, J.; Eichler, A.; Moser, J.; Ceballos, G.; Rurali, R.; Bachtold, A. A nanomechanical mass sensor with yoctogram resolution. *Nature nanotechnology* **2012**, *7*, 301–304.

(7) Guerra, D. N.; Bulsara, A. R.; Ditto, W. L.; Sinha, S.; Murali, K.; Mohanty, P. A noise-assisted reprogrammable nanomechanical logic gate. *Nano letters* **2010**, *10*, 1168–1171.

(8) Mahboob, I.; Flurin, E.; Nishiguchi, K.; Fujiwara, A.; Yamaguchi, H. Interconnect-free parallel logic circuits in a single mechanical resonator. *Nature communications* **2011**, *2*, 1–7.

(9) Karabalin, R.; Lifshitz, R.; Cross, M.; Matheny, M.; Masmanidis, S.; Roukes, M. Signal amplification by sensitive control of bifurcation topology. *Physical review letters* **2011**, *106*, 094102.

(10) Mahboob, I.; Yamaguchi, H. Bit storage and bit flip operations in an electromechanical oscillator. *Nature nanotechnology* **2008**, *3*, 275–279.

(11) Okamoto, H.; Gourgout, A.; Chang, C.-Y.; Onomitsu, K.; Mahboob, I.; Chang, E. Y.; Yamaguchi, H. Coherent phonon manipulation in coupled mechanical resonators. *Nature Physics* **2013**, *9*, 480–484.

(12) Faust, T.; Rieger, J.; Seitner, M. J.; Krenn, P.; Kotthaus, J. P.; Weig, E. M. Nonadiabatic dynamics of two strongly coupled nanomechanical resonator modes. *Physical review letters* **2012**, *109*, 037205.

(13) Bannon, F. D.; Clark, J. R.; Nguyen, C.-C. High-Q HF microelectromechanical filters. *IEEE Journal of solid-state circuits* **2000**, *35*, 512–526.

(14) Faust, T.; Rieger, J.; Seitner, M. J.; Kotthaus, J. P.; Weig, E. M. Coherent control of a classical nanomechanical two-level system. *Nature Physics* **2013**, *9*, 485–488.

(15) Mahboob, I.; Nishiguchi, K.; Okamoto, H.; Yamaguchi, H. Phonon-cavity electromechanics. *Nature Physics* **2012**, *8*, 387–392.

(16) Sun, F.; Dong, X.; Zou, J.; Dykman, M. I.; Chan, H. B. Correlated anomalous phase diffusion of coupled phononic modes in a sideband-driven resonator. *Nature communications* **2016**, *7*, 1–8.

(17) Faust, T.; Krenn, P.; Manus, S.; Kotthaus, J. P.; Weig, E. M. Microwave cavity-enhanced transduction for plug and play nanomechanics at room temperature. *Nature communications* **2012**, *3*, 1–6.

(18) Cattiaux, D.; Zhou, X.; Kumar, S.; Golokolenov, I.; Gazizulin, R.; Luck, A.; de Lépinay, L. M.; Sillanpää, M.; Armour, A.; Fefferman, A., et al. Beyond linear coupling in microwave optomechanics. *Physical Review Research* **2020**, *2*, 033480.

(19) Weis, S.; Rivière, R.; Deléglise, S.; Gavartin, E.; Arcizet, O.; Schliesser, A.; Kippenberg, T. J. Optomechanically induced transparency. *Science* **2010**, *330*, 1520–1523.

(20) Zeng, Q.; Zeng, K. Strong phonon-cavity coupling and parametric interaction in a single microcantilever under ambient conditions. *Journal of Physics D: Applied Physics* **2021**, *54*, 475307.

(21) Fan, L.; Fong, K. Y.; Poot, M.; Tang, H. X. Cascaded optical transparency in multimode-cavity optomechanical systems. *Nature communications* **2015**, *6*, 1–6.

(22) Shahidani, S.; Naderi, M.; Soltanolkotabi, M. Control and manipulation of electromagnetically induced transparency in a nonlinear optomechanical system with two movable mirrors. *Physical Review A* **2013**, *88*, 053813.

(23) Mahboob, I.; Perrissin, N.; Nishiguchi, K.; Hatanaka, D.; Okazaki, Y.; Fujiwara, A.; Yamaguchi, H. Dispersive and dissipative coupling in a micromechanical resonator embedded with a nanomechanical resonator. *Nano letters* **2015**, *15*, 2312–2317.

(24) Karabalin, R.; Cross, M.; Roukes, M. Nonlinear dynamics and chaos in two coupled nanomechanical resonators. *Physical Review B* **2009**, *79*, 165309.

(25) De Alba, R.; Massel, F.; Storch, I. R.; Abhilash, T.; Hui, A.; McEuen, P. L.; Craighead, H. G.; Parpia, J. M. Tunable phonon-cavity coupling in graphene membranes. *Nature nanotechnology* **2016**, *11*, 741–746.

(26) Šiškins, M.; Sokolovskaya, E.; Lee, M.; Mañas-Valero, S.; Davidovikj, D.; van der Zant, H. S. J.; Steeneken, P. G. Tunable strong coupling of mechanical resonance between spatially separated FePS3 nanodrums. *Nano letters* **2021**, *22*, 36–42.

(27) Huang, P.; Wang, P.; Zhou, J.; Wang, Z.; Ju, C.; Wang, Z.; Shen, Y.; Duan, C.; Du, J. Demonstration of motion transduction based on parametrically coupled mechanical resonators. *Physical Review Letters* **2013**, *110*, 227202.

(28) Zhou, X.; Venkatachalam, S.; Zhou, R.; Xu, H.; Pokharel, A.; Fefferman, A.; Zaknoune, M.; Collin, E. High-Q silicon nitride drum resonators strongly coupled to gates. *Nano Letters* **2021**, *21*, 5738–5744.

(29) Hocke, F.; Zhou, X.; Schliesser, A.; Kippenberg, T. J.; Huebl, H.; Gross, R. Electromechanically induced absorption in a circuit nano-electromechanical system. *New Journal of Physics* **2012**, *14*, 123037.

(30) Zhou, X.; Cattiaux, D.; Gazizulin, R.; Luck, A.; Maillet, O.; Crozes, T.; Motte, J.-F.; Bourgeois, O.; Fefferman, A.; Collin, E. On-chip Thermometry for Microwave Optomechanics Implemented in a Nuclear Demagnetization Cryostat. *Physical Review Applied* **2019**, *12*, 044066.

(31) Teufel, J. D.; Donner, T.; Li, D.; Harlow, J. W.; Allman, M.; Cicak, K.; Sirois, A. J.; Whittaker, J. D.; Lehnert, K. W.; Simmonds, R. W. Sideband cooling of micromechanical motion to the quantum ground state. *Nature* **2011**, *475*, 359–363.

(32) Pan, F.; Cui, K.; Bai, G.; Feng, X.; Liu, F.; Zhang, W.; Huang, Y. Radiation-pressure-antidamping enhanced optomechanical spring sensing. *ACS Photonics* **2018**, *5*, 4164–4169.

(33) Aspelmeyer, M.; Kippenberg, T. J.; Marquardt, F. Cavity optomechanics. *Reviews of Modern Physics* **2014**, *86*, 1391.

(34) Zhou, X.; Cattiaux, D.; Theron, D.; Collin, E. Electric circuit model of microwave optomechanics. *Journal of Applied Physics* **2021**, *129*, 114502.

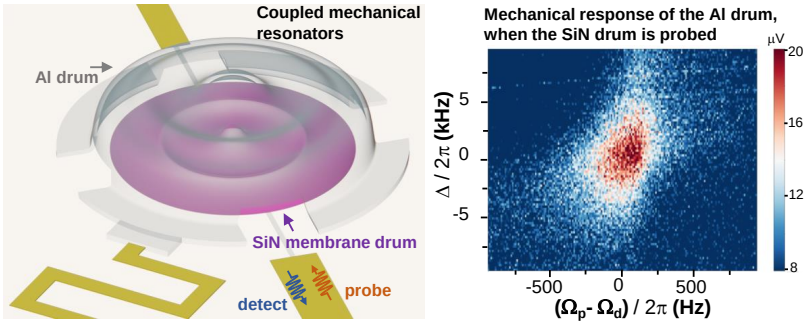
Coupled mechanical resonators
Al drum
SiN membrane drum
probe
detect
Mechanical response of the Al drum, when the SiN drum is probed
μV
20
16
12
8
Δ / 2π (kHz)
5
0
-5
-500
0
500
(Ωp- Ωd) / 2π (Hz)

Supporting Information: Coupling capacitively distinct mechanical resonators for room temperature phonon-cavity electromechanics

Alok Pokharel,[†] Hao Xu,[†] Srisaran Venkatachalam,[†] Eddy Collin,[‡] and Xin Zhou[*,†]

†*Univ. Lille, CNRS, Centrale Lille, Univ. Polytechnique Hauts-de-France, UMR 8520 - IEMN, F-59000 Lille, France*

‡*Univ. Grenoble Alpes, Institut NEEL - CNRS UPR2940, 25 rue des Martyrs, BP 166, 38042 Grenoble Cedex 9, France*

E-mail: CorrespondingAuthor:xin.zhou@cnrs.fr

Device fabrication and basic mechanical properties

The device, measured in this work, consists of a SiN membrane drum resonator capacitively coupled to an Al drum. The device fabrication process starts with a silicon substrate covered with a stoichiometric SiN thin film (80 nm in thickness) having $\sim$1 GPa tensile stress. Circularly symmetric holes, with 300 nm in diameter, are patterned on its top by using electron beam lithography. In order to release SiN drum from the substrate through these holes, reactive iron etching is used to remove the SiN layer, followed by a XeF_2 selective etching process to partly remove Si substrate. Then, about 25 nm Al thin film is deposited on SiN drum as a conductive layer. An Al drum resonator is fabricated by using PMMA (polymethyl methacrylate) resist as sacrifice layer through soft-bake and reflowed process.

The Al drum is patterned by using MMA (methyl methacrylate) and PMMA resist through using EB lithography, followed with Al deposition and lift-off process.[1]

To verify whether the plate or membrane model is suitable for our drums, we evaluate the ratio between the tension in the drum and its bending rigidity, $\sigma 2\pi hR/(D_r/R)$, where $\sigma 2\pi hR$ is the tension with the drum and $D_r = \frac{E_r h^3}{12(1-v^2)}$ is the flexural rigidity in the plane of the drum, v is the Poisson's ratio, h is the thickness of the film, $E_r$is Young's modulus, and R is the radius of the drum.[2,3] For the SiN drum, by using parameters of $\sigma \sim$ in the range from 0.8 GPa to 1.0 GPa, $R = 18$ μm, $h = 80$ nm, v ~0.3, $E_r = 240$ GPa (for SiN), the value of $\sigma 2\pi hR/(D_r/R)$ will be in the range from 1.1^4 to 1.4×10^4, exhibiting the tension-dominant property. Therefore, SiN drum follows membrane model. While, for our Al drum, it gives ~26 by using device parameters of $\sigma \sim 15$ MPa,[4] $R = 20$ μm, $h \sim 550$ nm, v ~0.3, and E_r = 69 GPa (for Al). Comparing with the SiN drum, this Al drum approaches to the plate model, but is still a membrane.

Analytical calculation for two-tone driving scheme

This simple device structure allows to consider two parametrically coupled electromechanical resonators as a single capacitor $C_g\left(X_1, X_2\right)$ consisting of two parallel and movable membranes. The mechanical displacement of each membrane is described by $X_1(t)$ and $X_2(t)$ resonating at the frequency Ω_1 and Ω_2, with $\Omega_1 > \Omega_2$. We therefore model these two coupled drums in the linear response regime, driven by an electrostatic force

$$F_{1,2}(t) = \frac{(V_{dc} + V_{ac})^2}{2} \frac{\partial}{\partial X_{1,2}} C_g\left(X_1, X_2\right), \tag{S.1}$$

via the following equations of motion for the displacement $X_1(t)$ and $X_2(t)$,

$$\ddot{X}_1 + \gamma_1 \dot{X}_1 + \Omega_1^2 X_1 = \frac{V_{ac} V_{dc}}{d\, m_1} C_{g0} \left[1 - \frac{2(X_2 - X_1)}{d}\right],$$
$$\ddot{X}_2 + \gamma_2 \dot{X}_2 + \Omega_2^2 X_2 = \frac{V_{ac} V_{dc}}{d\, m_2} C_{g0} \left[-1 + \frac{2(X_2 - X_1)}{d}\right]. \tag{S.2}$$

Here, the $\gamma_{1,2}$ is the mechanical damping rate, the $m_{1,2}$ is the effective mass, and C_{g0} is the initial capacitance between two membranes separated by a distance d. The driving force $F_{1,2}(t)$ is modeled as a simple parallel plate capacitor, and the force is truncated at the second order Taylor expansion of the $C_g(x)$, $\approx C_{g0}(1 - \frac{x}{d} + \frac{x^2}{d^2})$, with $x(t)$=$X_2(t) - X_1(t)$ In the Eq.S.2, an approximation $2V_{dc}V_{ac} + V_{ac}^2 \approx 2V_{dc}V_{ac}$ has been made by considering a general case in measurements: $V_{dc} \gg |V_{ac}|$. The static contribution V_{dc}^2 has been dropped of the equation since it cannot drive resonantly the modes; note however that this term can be employed to tune the resonance frequencies.[1] We shall not refer to this possibility in the present work.

To demonstrate phonon-cavity in a two-tone driving scheme, the membrane having the higher resonance frequency is chosen as phonon-cavity (with index 1). The other coupled mechanical resonator with the lower resonance frequency is marked with index 2. We exploit one driving tone with frequency Ω_d to weakly probe one of the coupled membranes around Ω_1 or Ω_2 and the other one with frequency Ω_p to pump the phonon-cavity at its sideband $\sim \Omega_1 \pm \Omega_2$. Therefore, we also write V_{ac} in the form of $V_{ac}(\omega_p, \omega_d) = \frac{\mu_p}{2} e^{-i\Omega_p t} + \frac{\mu_d}{2} e^{-i\Omega_d t} + c.c.$ The Eq.S.2 can be analytically solved in the rotating frame through looking for the displacement driven by the probe signal, $X_{1(2)}(t)$=$\frac{x_{1(2)}(t)}{2} e^{-i\Omega_d t} + c.c$ and the displacement of the other coupled membrane generated by the frequency mixing between the probe and the pump signals, $X_{2(1)}(t)$=$\frac{x_{2(1)}(t)}{2} e^{-i(\Omega_p \mp \Omega_d)t} + c.c.$ The $x_{1(2)}$ is the slowly varying complex amplitudes of mechanical displacements.

First, we drive the phonon-cavity at the frequency with small amplitude around its resonance frequency Ω_1 with the frequency detuning δ, Ω_d=Ω_1+δ. (a) Pump the photon-cavity at its red sideband with the frequency Δ detuned from Ω_1-Ω_2, Ω_p=Ω_1-Ω_2+Δ. Based

on an approximation that $\Omega_1^2 - \Omega_d^2 \approx 2\Omega_1(\Omega_1 - \Omega_d)$, the analytical solution of Eq.S.2 gives

$$\begin{aligned} x_1 &= \frac{f_d}{2m_1\Omega_1}\frac{1}{\frac{1}{\chi_1} - \frac{|f_p|^2\chi_2}{4m_1m_2d^2\Omega_1\Omega_2}}, \\ x_2 &= -\frac{f_p^*}{2m_2\Omega_2}\frac{x_1}{d}\chi_2 \end{aligned} \tag{S.3}$$

(b) For pumping the photon-cavity at its blue sideband at the frequency Ω_p=Ω_1+Ω_2+Δ, it arrives

$$\begin{aligned} x_1 &= \frac{f_d}{2m_1\Omega_1}\frac{1}{\frac{1}{\chi_1} + \frac{|f_p|^2\chi_2}{4m_1m_2d^2\Omega_1\Omega_2}}, \\ x_2^* &= \frac{f_p^*}{2m_2\Omega_2}\frac{x_1}{d}\chi_2 \end{aligned} \tag{S.4}$$

Here, we define the susceptibility of the phonon-cavity χ_1 and the mechanical susceptibility χ_2 corresponding to both red and blue sideband pumping the phonon-cavity.

$$\begin{aligned} \chi_1 &= \frac{1}{-\delta - i\frac{\gamma_1}{2}}, \\ \chi_2 &= \frac{1}{\Delta - \delta - i\frac{\gamma_2}{2}}, \end{aligned} \tag{S.5}$$

The $f_p = \frac{C_{g0}V_{dc}\mu_p}{d}$ and $f_d = \frac{C_{g0}V_{dc}\mu_d}{d}$ are complex amplitudes respectively corresponding to the pumping and driving force. To have analogues of optomechanical system, we define the coupling strength as $G = \frac{\partial\Omega_1}{\partial X_2} \approx \frac{\partial\Omega_1}{\partial C_g}\frac{\partial C_g}{\partial X_2} \approx$-$\frac{\Omega_1}{2d}$. It gives single phonon coupling strength g_0=$G\sqrt{\frac{\hbar}{2m_2\Omega_2}}$, where $\sqrt{\frac{\hbar}{2m_2\Omega_2}}$ is the zero-point fluctuations of the coupled membrane with resonance frequency Ω_2. Therefore, the term of $\frac{|f_p|^2}{4m_1m_2d^2\Omega_1\Omega_2}$ can be re-written as $n_pg_0^2$ through making a definition of the phonon number $n_p \approx \frac{2|f_p|^2}{m_1\Omega_1^2}\frac{1}{\hbar\Omega_p}$, generated by the pump tone. Then, Eq.S.4 becomes:

$$x_1 = \frac{f_d}{2m_1\Omega_1}\frac{1}{\chi_1^{-1} \pm n_pg_0^2\chi_2}, \tag{S.6}$$

where "-" and "+" symbols correspond to "red" and "blue" sideband pumping scheme.

Second, we probe the coupled membrane at the frequency around its resonance frequency Ω_2 with the frequency detuning δ, Ω_d=Ω_2+δ. Similarly, an approximation of $\Omega_2^2 - \Omega_d^2 \approx$

$2\Omega_2(\Omega_2 - \Omega_d)$ has been made. For pumping the photon-cavity at its red sideband, the analytical solution of Eq.S.2 gives

$$\begin{aligned} x_2 &= -\frac{f_d}{2m_2\Omega_2}\frac{1}{\chi_2^{-1} - n_p g_0^2 \chi_1}, \\ x_1 &= -\frac{f_p^*}{2m_1\Omega_1}\frac{x_2}{d}\chi_1, \\ \chi_1 &= \frac{1}{-\Delta - \delta - i\frac{\gamma_1}{2}}, \\ \chi_2 &= \frac{1}{-\delta - i\frac{\gamma_2}{2}}. \end{aligned} \tag{S.7}$$

For the blue sideband pumping, it arrives

$$\begin{aligned} x_2 &= -\frac{f_d}{2m_2\Omega_2}\frac{1}{\chi_2^{-1} - n_p g_0^2 \chi_1^*}, \\ x_1^* &= -\frac{f_p^*}{2m_1\Omega_1}\frac{x_2}{d}\chi_1^*, \\ \chi_1^* &= \frac{1}{\delta - \Delta + i\frac{\gamma_1}{2}}, \\ \chi_2 &= \frac{1}{-\delta - i\frac{\gamma_2}{2}}. \end{aligned} \tag{S.8}$$

Analytical calculation for single-tone sideband pumping scheme: analogy to optomechanical damping effect

Here, we define the phonon-cavity is sideband pumped at $\Omega_p = \Omega_1 + \beta$, where β is the frequency detuning from the resonance frequency of the phonon-cavity Ω_1. The mechanical displacement of the coupled membrane (with the index 2) is written as $x_2(t) = \frac{1}{2}\delta x_2(t)e^{-i\Omega_2 t} + c.c$, where the complex amplitude of $\delta x_2(t)$ is the Brownian motion of the the membrane(2).[5] The terms where motion $x_2(t)$ multiplies pump amplitude in Eq.S.2 generate harmonics at $\Omega_n = \Omega_p + n\Omega_2$, with n $\in \mathbb{Z}$. The solution can be found in the form of the *ansatz*,

$$x(t) = \sum_{n=-\infty}^{+\infty} \frac{\delta x(t)}{2} e^{-i(\Omega_p + n\Omega_2)t} + c.c. \tag{S.9}$$

In this work, we are interested only in schemes of $n = \pm 1$, corresponding to the "down" and "up" sideband of the pump signals at the frequency $\Omega_- = \Omega_p - \Omega_2$ and $\Omega_+ = \Omega_p + \Omega_2$. The solution of the phonon-cavity motion equation in Eq.S.2 is given by

$$\begin{aligned} x_- &= \frac{e^{-i\Omega_- t}}{2} \frac{f_p \delta x_2^*}{m_1 d} \frac{1}{\Omega_1^2 - \Omega_-^2 - i\Omega_- \gamma_1} + c.c, \\ x_+ &= \frac{e^{-i\Omega_+ t}}{2} \frac{f_p \delta x_2}{m_1 d} \frac{1}{\Omega_1^2 - \Omega_+^2 - i\Omega_+ \gamma_1} + c.c. \end{aligned} \tag{S.10}$$

It yields an extra force, $f_{cav} = \frac{f_p}{d} x_-^* + \frac{f_p^*}{d} x_+ + c.c$, biasing on the membrane(2), which modifies the initial mechanical susceptibility to become

$$\begin{aligned} \chi_2(\Omega) &= \frac{1}{2m_2\Omega_2} \frac{1}{(-\Omega - i\frac{\gamma_2}{2}) + \Sigma}, \\ \Sigma &= \frac{|f_p|^2}{4m_1 m_2 d^2 \Omega_1 \Omega_2} \left(\frac{\Omega_2 + \beta - i\frac{\gamma_1}{2}}{(\Omega_2 + \beta)^2 + \frac{\gamma_1^2}{4}} - \frac{\Omega_2 - \beta - i\frac{\gamma_1}{2}}{(\Omega_2 - \beta)^2 + \frac{\gamma_1^2}{4}} \right) \end{aligned} \tag{S.11}$$

The imaginary part of Σ modifies the mechanical damping rate γ_2, yielding additional damping γ_{opt}

$$\gamma_{opt} = n_p g_0^2 \left[\frac{\gamma_1}{(\Omega_2 + \beta)^2 + \frac{\gamma_1^2}{4}} - \frac{\gamma_1}{(\Omega_2 - \beta)^2 + \frac{\gamma_1^2}{4}} \right]. \tag{S.12}$$

The real part of Σ contributes to a frequency shift of Ω_2,

$$\delta\Omega_2 = -n_p g_0^2 \left[\frac{\beta + \Omega_2}{(\Omega_2 + \beta)^2 + \frac{\gamma_1^2}{4}} - \frac{\Omega_2 - \beta}{(\Omega_2 - \beta)^2 + \frac{\gamma_1^2}{4}} \right]. \tag{S.13}$$

Both expressions of Eq.S.12 and Eq.S.13 refer to "optical damping effect" and "optical spring effect" in optomechanics. The f_{cav} corresponds to the phonon-cavity force, originating from energy confined in the capacitor that consistsof two capacitively coupled membranes.

Using same method, we could get the dynamical backaction effects on the phonon-cavity,

$$\begin{aligned}\gamma_{opt(cavity)} &= n_p g_0^2 \left[\frac{\gamma_2}{(\Omega_2 - 2\Omega_1 - \beta)^2 + \frac{\gamma_2^2}{4}} - \frac{\gamma_2}{(\Omega_2 - \beta)^2 + \frac{\gamma_2^2}{4}} \right], \\ \delta\Omega_1 &= n_p g_0^2 \left[\frac{\Omega_2 - 2\Omega_1 - \beta}{(\Omega_2 - 2\Omega_1 - \beta)^2 + \frac{\gamma_2^2}{4}} + \frac{\Omega_2 - \beta}{(\Omega_2 - \beta)^2 + \frac{\gamma_2^2}{4}} \right].\end{aligned} \tag{S.14}$$

References

(1) Zhou, X.; Venkatachalam, S.; Zhou, R.; Xu, H.; Pokharel, A.; Fefferman, A.; Zaknoune, M.; Collin, E. High-Q silicon nitride drum resonators strongly coupled to gates. *Nano Letters* **2021**, *21*, 5738–5744.

(2) Lee, J.; Wang, Z.; He, K.; Shan, J.; Feng, P. X.-L. High frequency MoS2 nanomechanical resonators. *ACS nano* **2013**, *7*, 6086–6091.

(3) Cattiaux, D.; Kumar, S.; Zhou, X.; Fefferman, A.; Collin, E. Geometrical nonlinearity of circular plates and membranes: An alternative method. *Journal of Applied Physics* **2020**, *128*, 104501.

(4) Guisbiers, G.; Strehle, S.; Van Overschelde, O.; Wautelet, M. Residual Stresses in Ta, Mo, Al and Pd Thin Films Deposited by E-Beam Evaporation Process on Si and Si/SiO2 Substrates. AIP Conference Proceedings. 2006; pp 317–324.

(5) Zhou, X.; Cattiaux, D.; Theron, D.; Collin, E. Electric circuit model of microwave optomechanics. *Journal of Applied Physics* **2021**, *129*, 114502.